Available online at www.sciencedirect.com
SCIENCE DIRECT®
International Journal of Heat and Fluid Flow 25 (2004) 809–823
International Journal of HEAT AND FLUID FLOW
www.elsevier.com/locate/ijhff

The negatively buoyant turbulent wall jet: performance of alternative options in RANS modelling

T.J. Craft *, A.V. Gerasimov, H. Iacovides, J.W. Kidger, B.E. Launder

Department of Mechanical, Aerospace and Manufacturing Engineering, UMIST, P.O. Box 88, Manchester M60 1QD, UK

Accepted 21 May 2004
Available online 28 July 2004

Abstract

The paper describes the application of different levels of turbulence closure and near-wall treatment to the computation of a 2D downward-directed wall jet that encounters a slow, upward-moving flow. The working fluid is water and the two streams may be at the same temperature or the wall-jet fluid may be hotter, leading to significant buoyant effects. The distance of penetration of the wall jet is found to be highly dependent on the turbulence model employed. It is established first that the new analytical wall function (AWF) developed by the authors [Int. J. Heat Fluid Flow 23 (2002) 148] leads to flow predictions in close agreement with a so-called 'low-Reynolds-number' treatment where computations extend all the way to the wall. However, for some test cases, both sets of calculations (employing an eddy-viscosity model) indicate too great a penetration of the wall-jet into the opposing stream. The use of the AWF in conjunction with a second-moment closure, particularly one which satisfies the two-component-limit, gives generally closer agreement.

1. Introduction

In designing fail-safe cooling configurations for nuclear-reactor cores, a major concern is to develop a system that is unequivocally safe when a severe operational malfunction occurs, such as the failure of coolant-circulation pumps. If the pumps' operation should fail, highly complex flow patterns will ensue in which the flow becomes driven by buoyant forces. The ability to make accurate CFD simulations of such scenarios would help greatly in improving design. However, current industrial CFD modelling generally employs simple eddy-viscosity models, with wall-functions providing an economical bridge across the near-wall viscosity-affected sub-layer. The realism achieved by such a level of turbulence modelling for buoyancy-dominated and other complex flows is unreliable and often poor. A UK nuclear-power consortium has thus commissioned experiments, LES and CFD simulations of a number of geometrically simple but physically challenging mixed-convection flows to assess the capabilities of existing approaches and encourage development of more applicable modelling practices.

The above research programme has so far focused on flows along a vertical wall where the primary velocity direction is vertical (up or down) with the principal velocity gradient horizontal. For such an arrangement, even under strong buoyant effects, it has long been known (Cotton and Jackson, 1987) that a two-equation eddy viscosity scheme *can* give reasonable flow predictions provided the thickening or thinning of the viscous sub-layer is accounted for. But, the low-Reynolds-number model of Launder and Sharma (1974) used in Cotton and Jackson (1987) and in most subsequent work is computationally expensive as it requires a very fine near-wall mesh to resolve the viscous sub-layer, leading to slow convergence rates. The prohibitive cost of using such a model in computationally complex flows is a deterrent to its use in most industrial work. In an earlier phase of the current research, therefore, the authors directed attention at developing a more general set of wall functions where, *inter alia*, the buoyant terms in the mean momentum equation and their consequent impact on the turbulence dynamics was explicitly accounted for, Craft et al. (2002). Applications were made for buoyancy-modified up- and down-flow through

* Corresponding author. Tel.: +44-161-200-8728; fax: +44-161-200-3723.
E-mail address: tim.craft@umist.ac.uk (T.J. Craft).

0142-727X/$ - see front matter © 2004 Elsevier Inc. All rights reserved.
doi:10.1016/j.ijheatfluidflow.2004.05.003

pipes and annuli, the level of agreement with experiment being generally satisfactory and very similar to that achieved by the model of Launder and Sharma (1974) which required at least an order of magnitude more computer resources even for these computationally simple flows (Craft et al., 2002, 2003). In contrast, the use of standard wall functions in computing the same flows led to errors in the computed heat-transfer coefficient of typically 50% or more and to a great sensitivity of the resultant Nusselt number to the thickness of the near-wall cell over which the wall function was applied.

The present contribution considers a more complex flow than the cases noted above; one closer to the types of flow that might arise in a pump-failure scenario signalled at the start of this section. The cases considered involve the vertically downward flow of a wall jet into the path of a slow-moving, upward stream. The collision of these streams results in a stagnation of the wall jet and its turning to flow upstream. In some tests the wall jet fluid is hotter than that of the counterflowing stream, leading to buoyant as well as dynamic influences on the stagnation point position. The turbulent wall jet (even with an isothermal co-flowing or stationary external stream) is known to be a difficult flow to predict (Launder and Rodi, 1983; Kline et al., 1981; Craft and Launder, 2001b). These cited studies suggest that to obtain reasonable predictions one needs to solve transport equations for the Reynolds stresses rather than assume an isotropic eddy viscosity. Moreover, Craft and Launder (2001b) found that, even at that level of modelling, for the three-dimensional wall jet the results were highly dependent on modelling details that had little influence in many simple shear flows. With this background experience, we felt it appropriate to explore the performance of two second-moment closures as well as the usual k–ε linear eddy viscosity model. Section 2 summarizes the family of cases examined while Section 3 outlines the physical and numerical models employed in the simulations. The computational results themselves are presented in Section 4 which lead us to the conclusions and directions for further work given in Section 5.

2. The test flows and their computational representation

The experimental configuration is shown schematically in Fig. 1, and details are reported in He et al. (2002). On the right side of the vertical channel a downward directed warm jet of water emerges from a development passage 33 hydraulic diameters in length. In the numerical computations, fully developed channel flow profiles at a Reynolds number of 4000 were interpolated onto this jet inlet. Standard wall functions were adopted on all walls except the right hand one on which the wall jet develops. On this wall, where flow reversal occurs, one of three treatments was applied as noted in

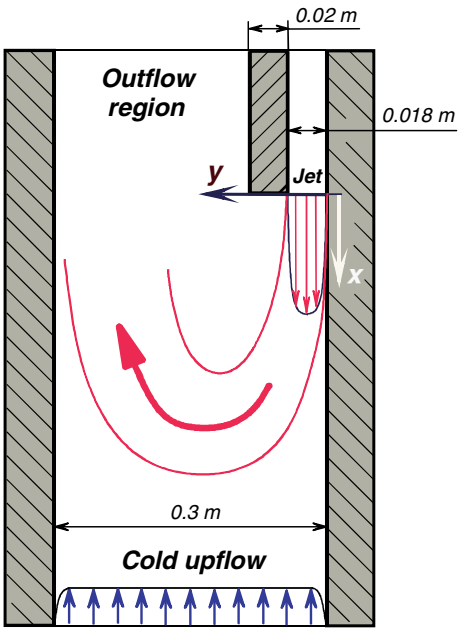

Fig. 1. Downward-directed opposed wall-jet flow.

Section 3. (For one test the analytical wall function [see Section 3.3] was also applied to the left-hand wall producing negligibly different results.) The walls were assumed to be adiabatic. The passage width (normal to the plane shown in Fig. 1) was 1.2 m giving an aspect ratio of 4:1 for the main passage. Although this ratio was rather small to assume flow two-dimensionality, some of the test-flows have also been the subject of an LES exploration by Addad et al. (2004), which supports the view that there were no serious departures from two-dimensionality in the experiments. An undeniable difficulty, however, was that the experimental inlet and exit profiles could not be measured. At the bottom there was a "flow-conditioning unit" suggesting a reasonably uniform entry profile should have been achieved with a rather high turbulence level. In the computations, therefore, uniform inlet velocity and turbulence-energy profiles were prescribed while the dissipation rate was set to give a turbulent viscosity 50 times the molecular value. The inlet turbulence was not a sensitive unknown however: a change in the inlet turbulence energy from 2% to 5% of the mean kinetic energy, had no discernible effect on the flow. For the isothermal tests the actual position of the lower inlet plane was set somewhat lower than in the experiments simply because the majority of the turbulence models employed did not cause the wall-jet to lose its momentum sufficiently rapidly. To prevent the imposed boundary conditions from enforcing the reversal of the wall jet we lowered the bottom of the computational domain to 1.3 m below the wall-jet injection point (rather than 1.0 m). As implied above, recent LES results reported in the companion paper (Addad et al., 2004) have removed many of the uncer-

tainties related to two-dimensionality and boundary conditions.

3. Mathematical and numerical models

3.1. Mean flow equations

In tensor notation the governing equations for the mean flow variables may be written as follows:

The continuity equation:

$$\frac{\partial(\rho U_j)}{\partial x_j} = 0 \tag{3.1}$$

The momentum equations:

$$\frac{\partial(\rho U_i U_j)}{\partial x_j} = -\frac{\partial P}{\partial x_i} + \frac{\partial}{\partial x_j}\left[\mu\left(\frac{\partial U_i}{\partial x_j} + \frac{\partial U_j}{\partial x_i}\right) - \rho\overline{u_i u_j}\right] + B_{Ti} \tag{3.2}$$

where $B_{Ti} = g_i(\rho - \rho_{\mathrm{ref}})$ is the buoyancy term. Instead of using the Boussinesq approximation, the state equation is written as $\rho - \rho_{\mathrm{ref}} = -\beta\rho_{\mathrm{ref}}(T - T_{\mathrm{ref}})$ and the effect of mean density variation has thus been retained in all the individual terms in Eqs. (3.1)–(3.3).

The energy equation:

$$\frac{\partial(\rho U_j T)}{\partial x_j} = \frac{\partial}{\partial x_j}\left[\frac{\mu}{Pr}\frac{\partial T}{\partial x_j} - \rho\overline{u_j t}\right] \tag{3.3}$$

The turbulent stresses, $\overline{u_i u_j}$, and the turbulent heat fluxes, $\overline{u_j t}$, are unknown in the above equations and are approximated by turbulence models as described below.

3.2. Turbulence models

Four turbulence models have been employed: the low-Reynolds-number linear k–ε eddy viscosity model (EVM) of Launder and Sharma (1974) and three high-Reynolds-number schemes (that is, models that need to be used with wall functions). These are:

- *The k–ε EVM without low-Reynolds-number terms*

The stresses and the turbulent heat fluxes in Eqs. (3.2), (3.3), (3.9) and (3.10) are modelled as

$$\rho\overline{u_i u_j} = \frac{2}{3}\rho k\delta_{ij} - \mu_t\left(\frac{\partial U_i}{\partial x_j} + \frac{\partial U_j}{\partial x_i}\right) \tag{3.4}$$

and

$$\rho\overline{u_i t} = -\frac{\mu_t}{Pr_t}\frac{\partial T}{\partial x_i} \tag{3.5}$$

The expression for the turbulent dynamic viscosity is as proposed by Jones and Launder (1972)

$$\mu_t = \rho c_\mu \frac{k^2}{\varepsilon} \tag{3.6}$$

The k-equation:

$$\frac{\partial(\rho U_j k)}{\partial x_j} = \frac{\partial}{\partial x_j}\left[\left(\mu + \frac{\mu_t}{\sigma_k}\right)\frac{\partial k}{\partial x_j}\right] + P_k + G_k - \rho\varepsilon \tag{3.7}$$

The ε-equation:

$$\frac{\partial(\rho U_j \varepsilon)}{\partial x_j} = \frac{\partial}{\partial x_j}\left[\left(\mu + \frac{\mu_t}{\sigma_\varepsilon}\right)\frac{\partial \varepsilon}{\partial x_j}\right] + c_{\epsilon 1}\frac{\varepsilon}{k}(P_k + G_k) - c_{\epsilon 2}\rho\frac{\varepsilon^2}{k} \tag{3.8}$$

The turbulent kinetic energy production due to the mean strain is

$$P_k = -\rho\overline{u_i u_j}\frac{\partial U_i}{\partial x_j} \tag{3.9}$$

and, in buoyant flows, there is an additional contribution to the generation rate of turbulence G_k, the exact expression of which can be written

$$G_k = \overline{\rho' u_i} g_i = -\rho\beta g_i \overline{u_i t} \tag{3.10}$$

where the density fluctuations ρ' in the turbulent density fluxes have been related to temperature fluctuations, t, by $\rho' = -\beta t$.

The constants and functions of the standard high-Reynolds-number k–ε model have the following values:

$c_\mu = 0.09$; $c_{\varepsilon 1} = 1.44$; $c_{\varepsilon 2} = 1.92$;

$\sigma_k = 1.0$; $\sigma_\varepsilon = 1.3$.

- *Second-moment closures*

Here two such closures have been employed, the "basic" closure of Gibson and Launder (1978) and the "two-component-limit" (TCL) closure of Craft and Launder (2001a). Both second-moment closures solve transport equations for each of the Reynolds stresses, $\overline{u_i u_j}$, in addition to that for ε.

The transport equation for the Reynolds stresses is of the form:

$$\frac{\mathrm{D}(\rho\overline{u_i u_j})}{\mathrm{D}t} = P_{ij} + G_{ij} + \phi_{ij} + d_{ij} - \rho\varepsilon_{ij} \tag{3.11}$$

where

$$P_{ij} = -\rho\left(\overline{u_i u_k}\frac{\partial U_j}{\partial x_k} + \overline{u_j u_k}\frac{\partial U_i}{\partial x_k}\right) \tag{3.12}$$

$$G_{ij} = \rho(\overline{f_i u_j} + \overline{f_j u_i}) = -\rho\beta(g_i\overline{u_j t} + g_j\overline{u_i t}) \tag{3.13}$$

$$\phi_{ij} = \overline{p\left(\frac{\partial u_i}{\partial x_j} + \frac{\partial u_j}{\partial x_i}\right)} \tag{3.14}$$

$$d_{ij} = -\frac{\partial}{\partial x_k}\left(\rho\overline{u_i u_j u_k} + \overline{pu_j}\delta_{ik} + \overline{pu_i}\delta_{jk} - \mu\frac{\partial\overline{u_i u_j}}{\partial x_k}\right) \tag{3.15}$$

$$\varepsilon_{ij} = -2\nu\overline{\frac{\partial u_i}{\partial x_k}\frac{\partial u_j}{\partial x_k}} \tag{3.16}$$

The generation rates due to shear, P_{ij}, and buoyancy, G_{ij}, do not require modelling. The turbulent transport

term, d_{ij}, is modelled through the generalized gradient diffusion hypothesis (GGDH) of Daly and Harlow (1970):

$$d_{ij} = \frac{\partial}{\partial x_k}\left(c_s \rho \frac{k}{\varepsilon} \overline{u_k u_l} \frac{\partial \overline{u_i u_j}}{\partial x_l} + \mu \frac{\partial \overline{u_i u_j}}{\partial x_k} \right) \tag{3.17}$$

where c_s is taken as 0.22.

Modelling of the dissipation rate ε_{ij} and the pressure-redistribution terms ϕ_{ij} is different for the two closures used in this study. The modelled expressions are given in full in Appendices C and D.

The equation for the turbulent kinetic energy dissipation rate, ε, is modelled using empirical and intuitive approaches similar to those used in the corresponding equation in k–ε schemes:

$$\frac{\mathrm{D}(\rho\varepsilon)}{\mathrm{D}t} = \frac{\rho\varepsilon^2}{k}\left(c_{\varepsilon 1} \frac{P_k + G_k}{\rho\varepsilon} - c_{\varepsilon 2} \right) + d_\varepsilon \tag{3.18}$$

where d_ε is modelled, using the GGDH, as

$$d_\varepsilon = \frac{\partial}{\partial x_k}\left(c_\varepsilon \rho \frac{k}{\varepsilon} \overline{u_k u_l} \frac{\partial \varepsilon}{\partial x_l} \right) \tag{3.19}$$

where $c_\varepsilon = 0.16$.

For the basic second-moment closure, the coefficients $c_{\varepsilon 1}$ and $c_{\varepsilon 2}$ are constants and have the values of 1.45 and 1.90 respectively.

An alternative form of the ε transport equation is used with the TCL second-moment closure, in which $c_{\varepsilon 1}$ is taken as 1.0 and $c_{\varepsilon 2}$ becomes a function of anisotropy invariants. The equation can, then, be written

$$\frac{\mathrm{D}(\rho\varepsilon)}{\mathrm{D}t} = \frac{\rho\varepsilon^2}{k}\left[\frac{P_k + G_k}{\rho\varepsilon} - \frac{1.9}{(1 + 0.7 A_2^{1/2} A)} \right] + d_\varepsilon \tag{3.20}$$

where A_2, A_3 are stress invariants and A is the so-called 'flatness' parameter which varies in magnitude from unity in isotropic turbulence to zero when fluctuations in one direction vanish, i.e. the 'two-component limit'

$$A = 1 - \frac{9}{8}(A_2 - A_3) \tag{3.21}$$

$$A_2 = a_{ij} a_{ij} \tag{3.22}$$

$$A_3 = a_{ij} a_{jk} a_{ki} \tag{3.23}$$

and a_{ij} is the stress anisotropy tensor

$$a_{ij} = \frac{\overline{u_i u_j}}{k} - \frac{2}{3}\delta_{ij} \tag{3.24}$$

One of the advantages of using Eq. (3.20) is that it produces significant improvements in the prediction of both the round jet and the 3D wall jet (see Craft, 1991; Craft and Launder, 2001b), amongst other flows.

In computing turbulent heat transport, when the eddy-viscosity models are used, a uniform turbulent Prandtl number of 0.9 is assumed, whereas with either of the second-moment closures we adopt the GGDH to model the kinematic turbulent heat flux, $\overline{u_i t}$:

$$-\overline{u_i t} = c_\theta (k/\varepsilon) \overline{u_i u_j} \partial T / \partial x_j \tag{3.25}$$

where c_θ is a constant taken as 0.30.

It should be noted that transport equations for the scalar flux $\overline{u_i t}$ and the scalar variance $\overline{t^2}$ have not been employed in this work. This is because the main focus of this study was a development of the near-wall modelling technique. At this stage we have thus used a much simpler representation of the turbulent heat fluxes $\overline{u_i t}$, in line with the approach often adopted.

Space constraints preclude further detailed descriptions of these models though each are reasonably well known to the modelling community and may readily be accessed through the indicated references.

3.3. Wall functions

Two approaches have been adopted, here termed the "standard" wall function and the "analytical wall function, AWF". The former is based on a form appropriate to an equilibrium, near-wall simple shear layer where turbulence generation and dissipation rates are in balance. In these circumstances, the wall-parallel velocity increases as the logarithm of distance from the wall:

$$U^* = (1/\kappa^*)\ln y^* + C$$
$$\text{where} \tag{3.26}$$
$$y^* \equiv y k^{1/2}/\nu \quad \text{and} \quad U^* \equiv \rho U k^{1/2}/\tau_w$$

and κ^* and C are supposedly constant. This is Spalding's generalized form of the *law of the wall*, the turbulence energy in Eq. (3.26) usually being evaluated at the near-wall node. Consistent approximations are made for the generation and dissipation rates of turbulence energy. These are shown in Appendix A.

In contrast, the analytical wall function approach is based on an assumed eddy viscosity distribution. While this scheme is documented in Craft et al. (2002), as it is new and relatively little known, a brief summary of the main features is given. Firstly, as indicated, the eddy viscosity distribution is assumed known. A simple form is adopted in which the turbulent viscosity across the wall-adjacent cell is zero over the viscous sub-layer of thickness y_v while beyond this it increases linearly with distance from the wall, Fig. 2:

$$\mu_t = 0 \quad \text{for } y^* \leqslant y_v^* \tag{3.27}$$

$$\frac{\mu_t}{\mu_v} = \alpha(y^* - y_v^*) = c_\mu c_l (y^* - y_v^*) \quad \text{for } y^* > y_v^* \tag{3.28}$$

where $y_v^* = 10.8$ is a dimensionless thickness of the zero-μ_t sub-layer. With this assumption, together with that of a uniform turbulent Prandtl number (of 0.9), it is possible to integrate the momentum and energy equations to obtain (complicated) analytical expressions for the mean temperature and velocity profiles that include the

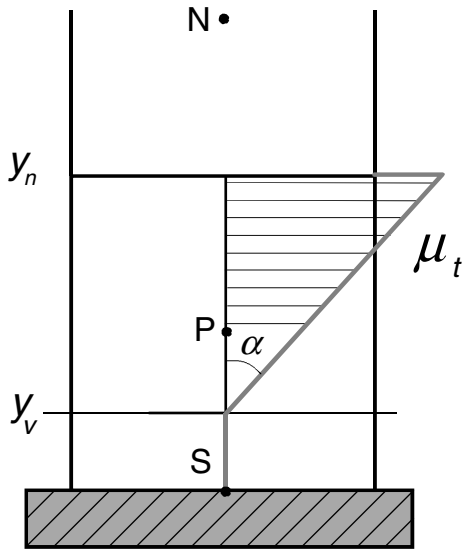

Fig. 2. Prescription of turbulent viscosity in the AWF.

effects of buoyancy in the streamwise velocity equation and a simple accounting of convective transport in both momentum and energy equations:

$$\frac{\partial(\rho UT)}{\partial x}+\frac{\partial(\rho VT)}{\partial y}=\frac{\partial}{\partial y}\left[\left(\frac{\mu}{Pr}+\frac{\mu_t}{Pr_t}\right)\frac{\partial T}{\partial y}\right] \tag{3.29}$$

$$\frac{\partial(\rho UU)}{\partial x}+\frac{\partial(\rho VU)}{\partial y}+\frac{\mathrm{d}P}{\mathrm{d}x}-g(\rho-\rho_{\mathrm{ref}})=\frac{\partial}{\partial y}\left[(\mu+\mu_t)\frac{\partial U}{\partial y}\right] \tag{3.30}$$

These equations are integrated across the near-wall control volume in two stages: first, across the sub-layer ($y^*\leqslant y_v^*$), where $\mu_t=0$, and then from the edge of the sub-layer over the rest of the near-wall cell. Boundary conditions are prescribed at the wall, and at the north cell face (Fig. 2) U and T values are obtained through interpolation between the two nodal values N and P on either side of the face. The analytical solutions can then provide values of the wall shear stress, and of either wall temperature or wall heat flux (depending upon the boundary condition) and of the average generation rate of k over the near-wall control volume.

In the k-equation, the turbulent kinetic energy is assumed to vary quadratically across the viscosity-dominated region in the immediate vicinity of the wall and to be uniform within the turbulent part of the near-wall cell. The diffusion of the turbulent kinetic energy to the wall is thus assumed to be zero. The production P_k and dissipation rate $\rho\varepsilon$ terms are represented by the average values of $\overline{P}_k$ and $\overline{\rho\varepsilon}$. The average generation rate term, $\overline{P}_k$, can be obtained via numerical integration of the following integral, using the analytically obtained expression for the shear strain $\partial U/\partial y^*$ and the prescribed profile of the turbulent viscosity (3.28):

$$\overline{P}_k=-\frac{1}{y_n}\int\mu_t\left(\frac{\partial U}{\partial y}\right)^2\mathrm{d}y=\frac{1}{y_n}\frac{\rho\sqrt{k_P}}{\mu}\int_{y_v^*}^{y_n^*}\mu\alpha(y^*-y_v^*)\left(\frac{\partial U}{\partial y^*}\right)^2\mathrm{d}y^* \tag{3.31}$$

The way that $\overline{\varepsilon}$, the space mean dissipation rate of k is prescribed across the near-wall control volume has also been revised. In the standard wall function, Chieng and Launder (1980), the dissipation rate across the near-wall control volume is assumed to vary according to

$$\varepsilon=\frac{2\nu k_P}{y_v^2}\quad\text{for } y^*\leqslant y_v^* \tag{3.32}$$

$$\varepsilon=\frac{k_P^{3/2}}{c_l y}\quad\text{for } y^*>y_v^* \tag{3.33}$$

where now $y_v^*=20$.

The above approach leads to a discontinuity in ε at $y=y_v$ with the maximum value of ε lying on the "turbulent" side of this interface. Here, in order to remove the discontinuity in the ε variation and to move the location of maximum ε to the wall the following variation is adopted:

$$\varepsilon=\frac{2\nu k_P}{y_d^2}\quad\text{for } y^*\leqslant y_d^* \tag{3.34}$$

$$\varepsilon=\frac{k_P^{3/2}}{c_l y}\quad\text{for } y^*>y_d^* \tag{3.35}$$

where $y_d^*=5.1$.

This strategy makes the introduction of further refinements possible. A crucial element of near-wall turbulence in conditions far from equilibrium is that the dimensionless sub-layer thickness y_v^* is by no means a universal constant (as most textbooks and even research papers still assume). Broadly, when the shear stress parallel to the wall decreases rapidly with distance from the wall, y_v^* becomes larger than its uniform-stress equilibrium level; and when the shear stress rises, y_v^* decreases. Originally it had been intended to include in the AWF a correlation for y_v^* in terms of the ratio of the shear stress at the wall to that at the edge of the viscous sub-layer, (τ_w/τ_v). That proved to be numerically unstable, however. Instead, we have achieved the same effect by letting the dissipation rate over the near-wall cell depend on this ratio of shear stresses. There are several other novel features to this AWF, including the accounting for changes in molecular properties across the sub-layer, the handling of Prandtl numbers significantly different from unity and the more accurate evaluation of wall-parallel momentum and enthalpy convective fluxes for the near-wall control volumes. Details of these and other features are given in Craft et al. (2002).

The addition of the Reynolds-stress transport equations requires some extension of the wall-function approach and commonly adopted practices are used, similar to those employed in the k-equation.

The diffusion of the normal stresses at the wall is taken to be zero, whilst terms in P_{ij} and ϕ_{ij} associated with the mean shear $\partial U/\partial y$ are replaced by cell-averaged values in a similar way to that adopted for P_k in the k-equation. The commonly adopted practice of setting the cell-averaged dissipation rate of the normal stresses to be isotropic:

$$\rho\varepsilon_{ij} = \frac{2}{3}\rho\overline{\varepsilon} \tag{3.36}$$

is also followed.

Because of the staggered grid arrangement employed here, the turbulent shear stress is treated differently from the normal stresses and its wall value is simply set equal to the wall shear stress.

Although the resulting AWF expressions, given in Appendix B, are complex, the overall computing time is similar to that of the standard wall functions as only extra analytical formulae are employed. This still gives computational savings of an order of magnitude or more in comparison to the LRN formulation.

3.4. Numerical solver

Computations have been carried out using the in-house TEAM code (Huang and Leschziner, 1983). It is a finite-volume code that employs the SIMPLE pressure correction algorithm in a staggered grid arrangement. The third-order QUICK scheme was used for the discretization of the convective transport of the mean flow variables and the PLDS scheme for the turbulence equations. For computations with the low-Reynolds-number model the grids employed were as fine as 130×280, and 130×300 for isothermal and non-isothermal flows respectively, while for the high-Reynolds-number model (using the 'analytical' and 'standard' wall functions) the corresponding finest meshes employed were 102×280 and 102×300. For the isothermal cases the computational domain started 0.4 m above the splitter plate and extended to 1.3 m below. For the non-isothermal cases the corresponding lengths were 2.4 and 0.6 m. These lengths were necessary to ensure that the resulting computations were not affected by the locations of the upper and lower boundaries.

4. Comparison of CFD results with test data

4.1. Isothermal flow

The non-buoyant tests enable the functioning of different parts of the modelling process to be distinguished while retaining the type of strain field prevailing under buoyancy-modified conditions. Comparisons of the mean velocity profile obtained from the LES (Addad et al., 2004) with the various closure results are shown in Fig. 3.

Note first, focusing on the contours on the right of each part of the figure, that the low-*Re* k–ε EVM produces a distinctly too large jet penetration (by about 30%) compared with the LES. Moreover, when this low-*Re* treatment is replaced by standard wall functions, the penetration depth of the wall jet increases by a further 30%. This result is superficially surprising since the review of two-dimensional wall jet spreading rates by Launder and Rodi (1981) indicated that, in the absence of an external stream, eddy viscosity models tended to

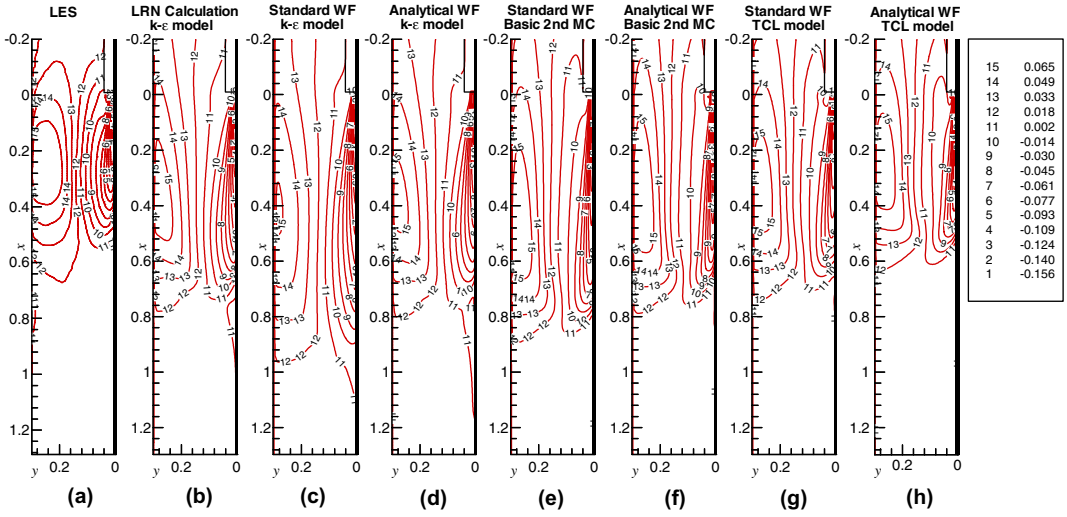

Fig. 3. Calculated vertical velocity contour plots for isothermal case $U_{ch}/U_{jet} = 0.077$.

predict a *too rapid wall-jet growth rate*, a result opposite from the behaviour shown in Fig. 3. We note next that if the standard wall function is replaced by the AWF the penetration depth reduces to practically the same level as that returned by the low-*Re* k–ε model. This confirms the behaviour reported in Craft et al. (2002, 2003), namely that the AWF mimics the low-*Re* model with admirable fidelity. Of course, unlike those earlier comparisons, in the present case neither model agrees closely with the target data.

Switching to second-moment closure brings a noticeable improvement: not only is the depth of penetration reduced; the shape of the contours is also generally improved, particularly near the stagnation point. But, with the 'basic' model used with the AWF, the wall jet still penetrates further than indicated by the LES. Only with the use of the TCL version together with the AWF is the penetration behaviour captured with satisfactory accuracy.

Fig. 4 compares velocity profiles across the wall jet at two depths. Both experimental and LES data are here included. It is clear that, while not perfect, the TCL–AWF modelling combination gives a reasonable account of the wall jet's development. The loss of the wall-jet's downward momentum arises principally from entrainment of fluid into the outer layer of the wall jet (reducing the level of the downward velocity) accompanied by a strongly rising pressure in the downward direction. We note from the velocity field vector plots, Fig. 5, that the TCL closure *does* show strong entrainment of fluid into the jet outer layer, which starts above the jet entry and continues several diameters below. The k–ε predictions on the other hand show very little entrainment, which explains why the TCL closure results in a more rapid thickening of the wall jet than the k–ε scheme. The experimental vector plots, Fig. 5(a) also show strong entrainment of external fluid, but in contrast to the TCL predictions, it is confined to the region immediately below the jet exit. The extra entrainment means that the TCL wall jet is less able to withstand the strong adverse pressure gradient, Fig. 6(a). A further

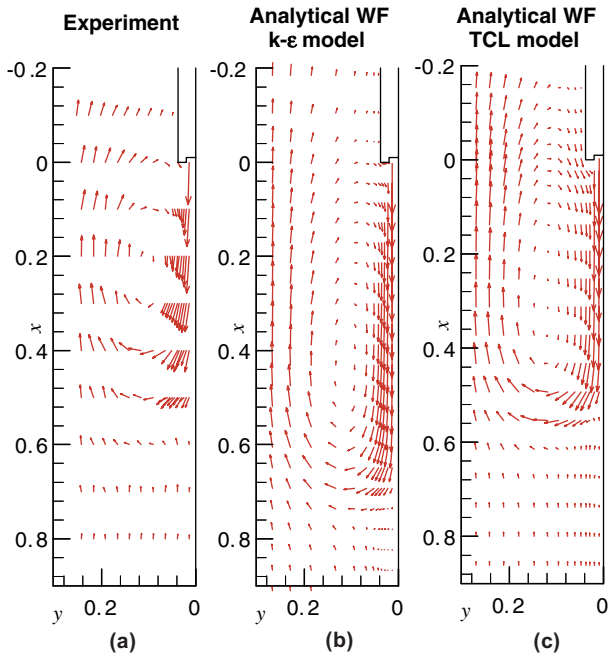

Fig. 5. Predicted vector plots for the isothermal case at $U_{ch}/U_{jet} = 0.077$.

contributing factor to the loss of the wall jet's momentum is the wall friction. We note in Fig. 6(b) that, for the first 0.4 m downstream from discharge, the TCL closure gives a friction factor that, on average, is 25% higher than the k–ε scheme. Comparisons with LES predictions of the friction factor, shown in Fig. 6(b), indicate that there is very close agreement between the LES and TCL–AWF computations especially for the first 0.4 m downstream of the discharge.

4.2. Buoyant cases

Attention is now turned to the buoyant flow test cases. For the case with the weaker upflow ($U_{ch}/U_{jet} = 0.077$), converged numerical solutions were only possible for the EVMs, while for the stronger upward flow

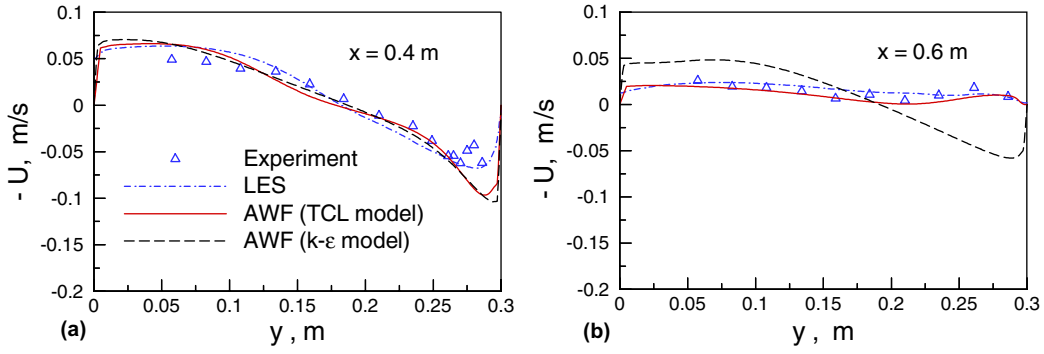

Fig. 4. Vertical velocity profiles at different locations x from jet discharge in isothermal case at $U_{ch}/U_{jet} = 0.077$.

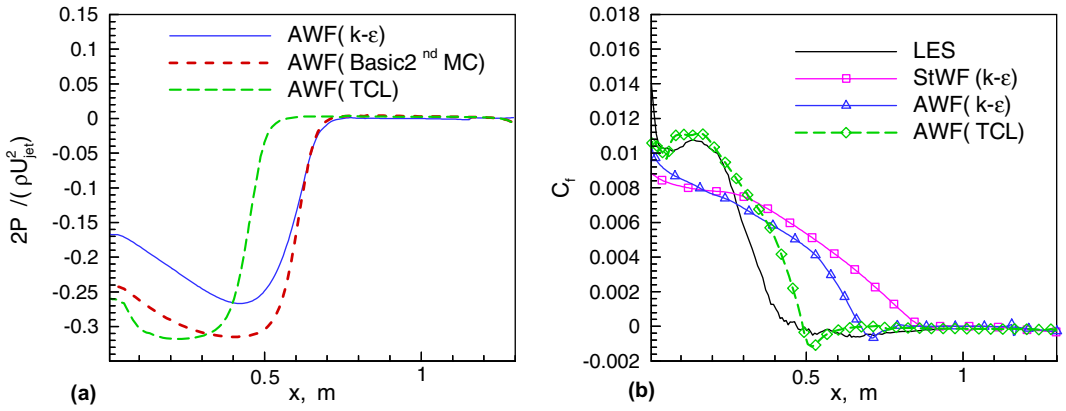

Fig. 6. Predicted distributions of (a) static pressure and (b) friction coefficient in the isothermal case at $U_{ch}/U_{jet} = 0.077$.

($U_{ch}/U_{jet} = 0.15$) computations have been obtained with all models. With the same upward velocity as in Section 4.1 ($U_{ch}/U_{jet} = 0.077$) the jet now penetrates only to a depth of 0.23m below its discharge point, which is only about 30% of that found in the isothermal case, Fig. 7(a). There is much less difference between models than in the isothermal flow; all models display a slightly greater penetration than the experiment, with the 'Standard' WF treatment proceeding furthest. Note, however, that the 'bulb' formed as the jet reverses is narrower for this treatment than for the other models. Moreover, the isotherm shape with 'Standard' WFs, Fig. 7(b), is much different in the region where the wall jet turns. These differences in the thermal field are solely due to differences in the dynamic wall boundary-condition treatment; for the thermal field a zero-gradient was simply applied in all cases. It is worth noting that here, too, the AWF predicts virtually the same result as the low-*Re* k–ε model. Finally, we note that despite these differences, all the schemes give the horizontal stably stratified front occurring at the same height, at x approximately equal to −0.15.

As the channel inlet velocity is increased the effects of buoyancy are weakened somewhat. For $U_{ch}/U_{jet} = 0.15$, as is shown in the temperature contours of Figs. 8 and 9, the penetration length is reduced to about 0.1 m and this is well reproduced by both the low-*Re* k–ε and the high-*Re* models with the AWF treatment; but the 'Standard' WF versions of both the high-*Re* k–ε and the Basic RSM models produce hardly any difference in thermal penetration from the previously discussed case. Both the LES and the limited experimental temperature contours, suggest that as the jet turns upwards it also spreads across the channel. With the k–ε and Basic RSM predictions, on the other hand, after turning the jet remains confined to the right hand side of the channel, moving upwards along the splitter plate. The TCL model computations, in closer agreement with the LES simulations, show that the jet moves further across the channel as it turns. The TCL–AWF predictions are again closer to

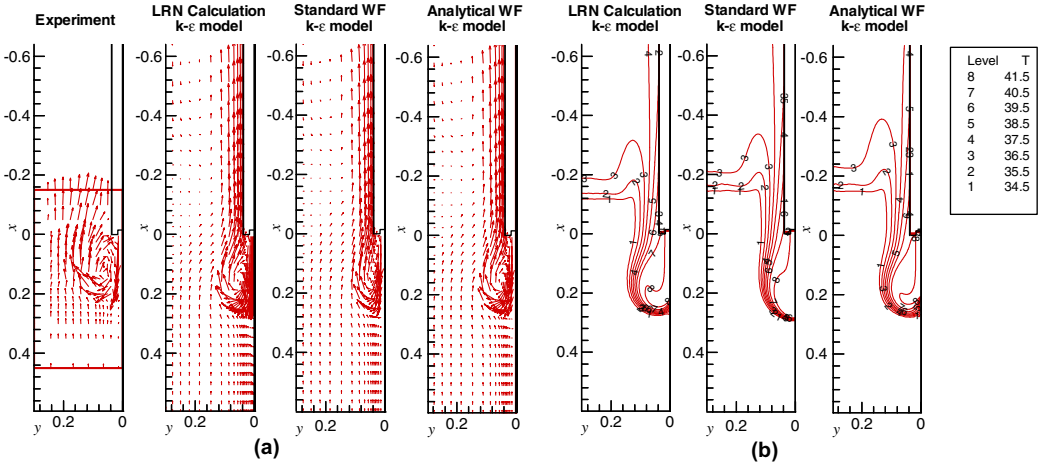

Fig. 7. Vector plots and temperature contours for the buoyant case at $U_{ch}/U_{jet} = 0.077$.

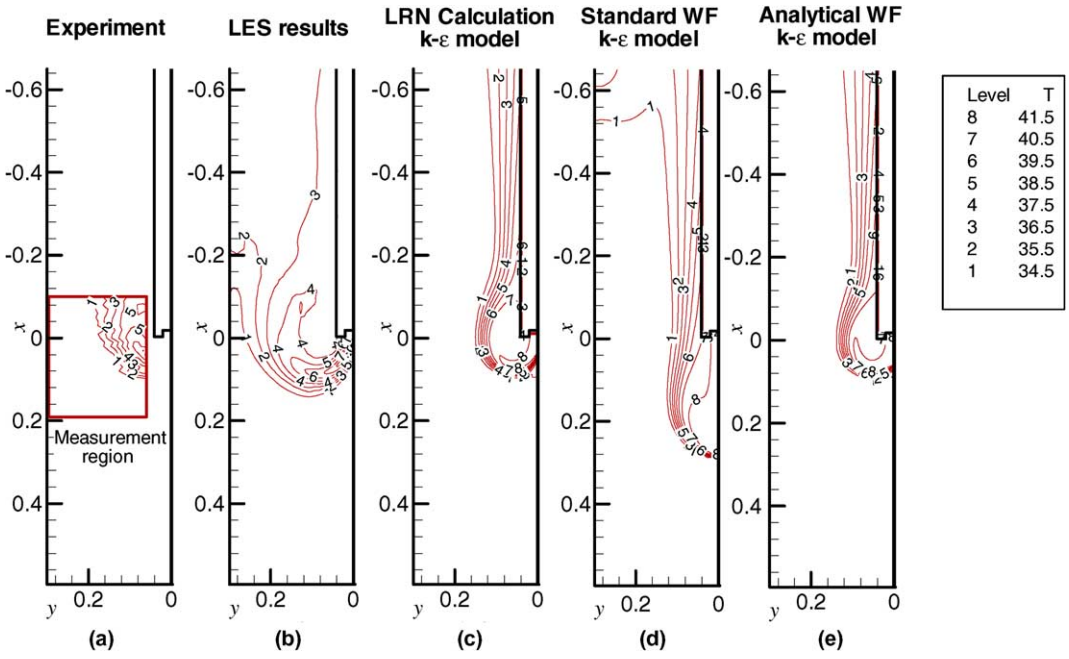

Fig. 8. Experimental, LES and EVM temperature contour plots for buoyant case at $U_{ch}/U_{jet} = 0.15$.

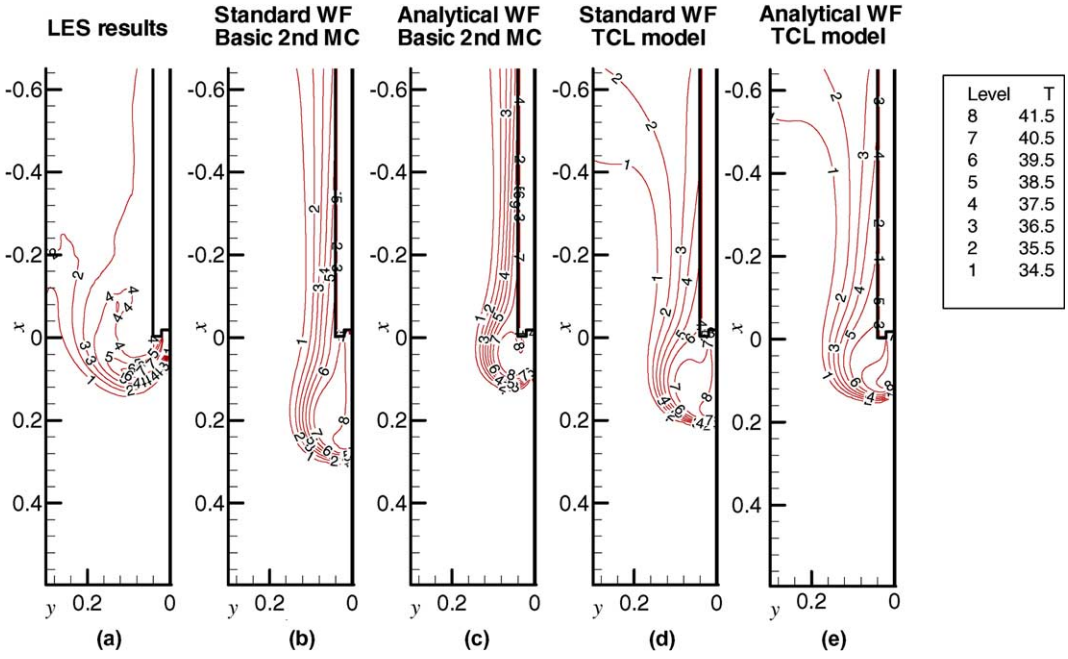

Fig. 9. LES and RSM temperature contour plots for buoyant case at $U_{ch}/U_{jet} = 0.15$.

the LES and experimental data than those of the TCL–StWF, notably in regard to the jet penetration.

The vector-plot comparisons of Fig. 10 also underline the differences among the different modelling strategies. They also show that in the TCL computations the near-wall modelling is not as influential as in the k–ε and basic RSM predictions.

5. Conclusions

The downward-directed, buoyancy-modified wall jet is a challenging flow to predict since apparently small modifications to the treatment of turbulence near boundaries can have a major effect on the resultant flow field. As in earlier tests on simpler pipe and annular

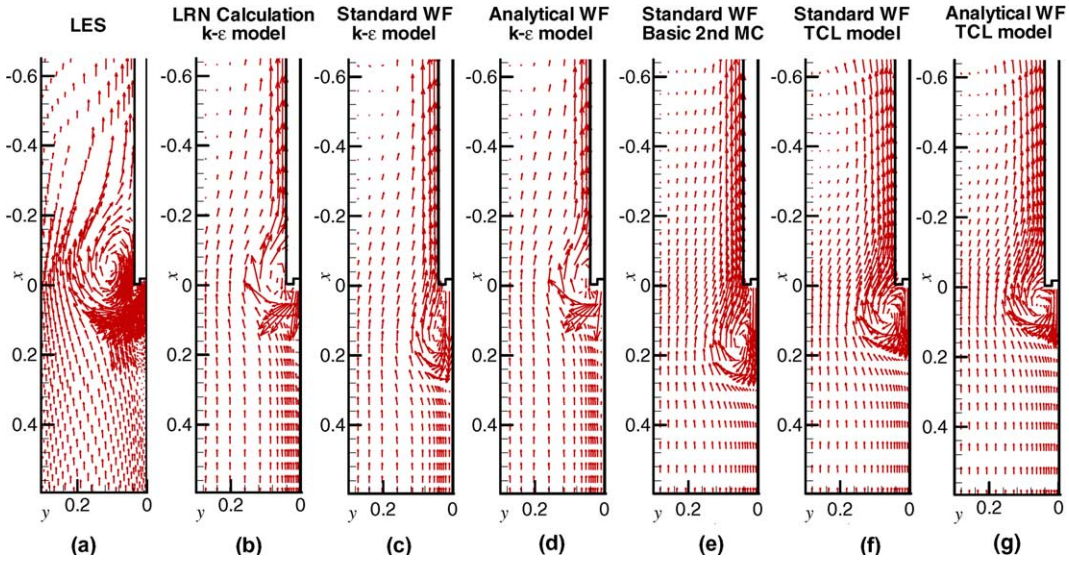

Fig. 10. Velocity vector plots for the buoyant case at $U_{ch}/U_{jet} = 0.15$.

flows, the Analytical Wall Function has returned results in very close agreement with the predictions obtained from the low-*Re* scheme. This is encouraging as the computing cost of using the AWF scheme is at least an order of magnitude less than the low-*Re*-number k–ε model.

A detailed study has been carried out on the non-buoyant opposed wall jet and one of the buoyant cases. This has shown that the two-component-limit (TCL) second-moment closure used with the AWF leads to very satisfactory agreement with the LES as well as with the available experimental data of these flows. However, numerical problems have so far prevented our securing fully-converged results for one of the two buoyant test cases (with the weaker upflow) using second-moment closure. This serves to underline that applying models at this level to a new type of flow may not infrequently throw up unforeseen impediments.

Bearing in mind that *horizontal* buoyant flows create even more severe modelling challenges than vertical ones, we recommend that future CFD development for reactor-safety and similar problems should be focused on the TCL second-moment closure employing a wall-function approach similar to that exemplified by the AWF.

Acknowledgements

The research has been sponsored through a consortium of UK nuclear energy companies coordinated by British Energy plc. We express our thanks to Dr M. Rabbitt of British Energy for his sympathetic monitoring of the programme. Authors' names are listed alphabetically.

Appendix A. Standard wall-function approach

In a conventional wall-function treatment:

1. The first near-wall grid node is placed far enough away from the wall at a distance y_P to be situated in the fully turbulent inner region.
2. The flow over this region is assumed to obey the semi-logarithmic law of the wall.
3. The local equilibrium conditions are then used to estimate the wall shear stress and also to evaluate the source terms in the turbulence transport equations (for k and other variables, depending on the model used).

Thus, in the near-wall control volume, for the velocity component parallel to the wall, the wall shear stress is commonly obtained from the following inversion and generalization of the log-law (Launder and Spalding, 1974):

$$\tau_{\text{wall}} = \frac{\kappa c_\mu^{1/4} \rho k_P^{1/2} U_P}{\ln(E c_\mu^{1/4} y_P^*)} \tag{A.1}$$

The above expression for the wall shear stress is then adopted in accounting for the forces applied to the near-wall control volume, for the velocity component parallel to the wall. When integrating the k transport equation for the near-wall cell:

1. Viscous transport of k to the wall is zero.
2. Because of their very rapid variation near the wall, the source terms in the k equation, P_k and ε, should not be assumed uniform over the near-wall control volume as is the usual practice with the internal cells.

These two terms are instead evaluated through analytical integration. We summarize below the type of strategy conventionally adopted.

A.1. Calculation of near-wall P_k

The starting point is the assumption that in the near-wall cell turbulence energy generation is by simple shear:

$$P_k = -\rho\overline{uv}\frac{\partial U}{\partial y} \tag{A.2}$$

From the local equilibrium conditions:

$$-\rho\overline{uv} = \tau_{\text{wall}} \quad \text{and}$$

$$U = \frac{\tau_{\text{wall}}}{\kappa c_\mu^{1/4}\rho k_P^{1/2}}\ln\left(E\frac{y k_P^{1/2}}{\nu}\right) \Rightarrow \frac{\partial U}{\partial y} = \frac{\tau_{\text{wall}}}{\kappa c_\mu^{1/4}\rho k_P^{1/2} y}$$

Thus

$$P_k = \frac{\tau_{\text{wall}}^2}{\kappa c_\mu^{1/4}\rho k_P^{1/2} y} \tag{A.3}$$

The above expression already contains the assumption that the turbulent shear stress remains constant over the control volume ($=\tau_{\text{wall}}$). Also, by setting k constant ($=k_P$), P_k can be integrated over the control volume. The integration is not, however, carried out over the entire control volume. The near-wall cell is subdivided into two layers: the fully turbulent region, away from the wall and the viscous layer next to the wall. P_k is assumed to be zero within the viscous layer. The edge of the sublayer is taken to be at a distance y_v from the wall, where $y_v k_P^{1/2}/\nu = 20$. Then the average P_k over the near-wall cell is obtained from:

$$\begin{aligned}\overline{P}_k &= \frac{1}{y_n}\int_{y_v}^{y_n}\frac{\tau_{\text{wall}}^2}{\kappa c_\mu^{1/4}\rho k_P^{1/2} y}\,\mathrm{d}y \\ &= \frac{\tau_{\text{wall}}^2}{\kappa c_\mu^{1/4}\rho k_P^{1/2} y_n}\ln\left(\frac{y_n}{y_v}\right)\end{aligned} \tag{A.4}$$

A.2. Calculation of near-wall dissipation rate

Over the fully turbulent layer $\varepsilon = k_P^{3/2}/(c_l y)$. Within the viscous sublayer, ε is assumed to remain constant and is evaluated at the edge of the sublayer as: $\varepsilon_v = k_P^{3/2}/(c_l y)$. Integration then leads to

$$\begin{aligned}\overline{\varepsilon} &= \frac{1}{y_n}\left[y_v\frac{k_P^{3/2}}{c_l y_v} + \int_{y_v}^{y_n}\frac{k_P^{3/2}}{c_l y}\,\mathrm{d}y\right] \\ &= \frac{1}{y_n}\left[y_v\frac{k_P^{3/2}}{c_l y_v} + \frac{k_P^{3/2}}{c_l y}\ln\left(\frac{y_n}{y_v}\right)\right]\end{aligned} \tag{A.5}$$

The transport equation for ε is not solved over the near-wall control volumes. The value of ε at the near-wall node is instead prescribed as

$$\varepsilon_P = \frac{k_P^{3/2}}{c_l y_P} \tag{A.6}$$

Appendix B. Analytical wall-function formulae

The near-wall molecular viscosity variation is assumed to be described by

$$\mu = \frac{\mu_{\text{wall}}}{1 + b_\mu y^*(y^* - 2y_v^*)} \tag{B.1}$$

where

$$b_\mu = \frac{1}{y_v^{*2}}\left(1 - \frac{\mu_{\text{wall}}}{\mu_v}\right) \tag{B.2}$$

The corresponding turbulent viscosity variation is held to vary as

$$\mu_t = \mu_v\alpha(y^* - y_v^*), \quad \text{where } \alpha = c_\mu c_l$$

With the above inputs the following resultant expressions are obtained:

- wall temperature

$$\begin{aligned}T_{\text{wall}} = T_n - \frac{Pr}{\mu_v\alpha_t}\Bigg\{&C_{\text{th2}}(y_n^* - y_v^*) + \left[\frac{\mu_v}{\mu_{\text{wall}}}(1 - b_\mu y_v^{*2})\right. \\ &\left.\times(C_{\text{th1}}y_v^* + A_{\text{th1}}) - \frac{C_{\text{th2}}}{\alpha_t}\right]\ln Y_{Tn}\Bigg\} \\ &- \frac{Pr y_v^*}{\mu_{\text{wall}}}\left[\frac{C_{\text{th1}}y_v^*}{2}\left(1 - b_\mu\frac{5y_v^{*2}}{6}\right)\right. \\ &\left.+ A_{\text{th1}}\left(1 - b_\mu\frac{2y_v^{*2}}{3}\right)\right]\end{aligned} \tag{B.3}$$

- wall shear stress

$$\tau_{\text{wall}} = -\frac{\rho_v\sqrt{k_P}}{\mu_v}\frac{\mu_v U_n - N}{\frac{\mu_v}{\mu_{\text{wall}}}\left[(1 - b_\mu y_v^{*2})\frac{\ln Y_n}{\alpha} + y_v^*\left(1 - b_\mu\frac{2y_v^{*2}}{3}\right)\right]} \tag{B.4}$$

- average production of turbulent kinetic energy

$$\overline{P}_k = \frac{1}{y_n}\frac{\rho_v\sqrt{k_P}}{\mu_v}\int_{y_v^*}^{y_n^*}\mu_v\alpha(y^* - y_v^*)\left(\frac{\partial U_2}{\partial y^*}\right)^2\mathrm{d}y^* \tag{B.5}$$

- average dissipation rate of turbulent kinetic energy across the near-wall cell

$$\overline{\varepsilon} = \frac{1}{y_n}\left[\frac{2k_P^{3/2}}{y_d^*} + \frac{k_P^{3/2}}{2.55}\ln\left(\frac{y_n}{y_d}\right)\right] \tag{B.6}$$

- average buoyant force across the near-wall control volume

$$\overline{F_b} = \beta'\left[\int_0^{y_v^*}(T_1' - T_{\mathrm{ref}})\,\mathrm{d}y^* + \int_{y_v^*}^{y_n^*}(T_2' - T_{\mathrm{ref}})\,\mathrm{d}y^*\right]$$
$$= \beta'\left[\left(\frac{T_{\mathrm{wall}} + T_v}{2} - T_{\mathrm{ref}}\right)y_v^* + \left(\frac{T_v + T_n}{2} - T_{\mathrm{ref}}\right)\left(y_n^* - y_v^*\right)\right] \quad \text{(B.7)}$$

where

$$A_{\mathrm{th1}} = -\frac{q_{\mathrm{wall}}}{c_p}\frac{\mu_v}{\rho_v\sqrt{k_P}} \quad \text{(B.8)}$$

$$\frac{\partial U_2}{\partial y^*} = \frac{1}{\mu_v Y}\left[C_2 y^* + A_2 + b(T_v - T_{\mathrm{ref}} + \delta T_y y_v^*)y^* - b\frac{\delta T_y}{2}y^{*2}\right] \quad \text{(B.9)}$$

$$A_2 = \frac{\mu_v}{\mu_{\mathrm{wall}}}C_1 y_v^*(1 - b_\mu y_v^{*2}) - C_2 y_v^* + \frac{\mu_v}{\mu_{\mathrm{wall}}}b(T_{\mathrm{wall}} - T_{\mathrm{ref}})y_v^*(1 - b_\mu y_v^{*2}) - \frac{\mu_v}{\mu_{\mathrm{wall}}}\frac{b(T_{\mathrm{wall}} - T_v)y_v^*}{2}(1 - b_\mu y_v^{*2}) - b\left(T_v - T_{\mathrm{ref}} + \frac{\delta T_y}{2}y_v^*\right)y_v^* + \frac{\mu_v U_n - N}{\left[(1 - b_\mu y_v^{*2})\frac{\ln Y_n}{\alpha} + y_v^*\left(1 - b_\mu\frac{2y_v^{*2}}{3}\right)\right]}(1 - b_\mu y_v^{*2}) \quad \text{(B.10)}$$

$$N = \frac{C_2}{\alpha}\left(y_n^* - y_v^* - \frac{1}{\alpha}\ln Y_n\right) + b\frac{(T_v - T_{\mathrm{ref}} + \delta T_y y_v^*)}{\alpha} \times \left[y_n^* - \left(\frac{1}{\alpha} - y_v^*\right)\ln Y_n\right] - b\frac{\delta T_y}{2\alpha}\left[\frac{y_n^{*2}}{2} - y_n^*\left(\frac{1}{\alpha} - y_v^*\right) + \left(\frac{1}{\alpha} - y_v^*\right)^2\ln Y_n\right] - \frac{by_v^*}{\alpha}\left[T_v - T_{\mathrm{ref}} + \frac{\delta T_y}{2}\left(\frac{y_v^*}{2} + \frac{1}{\alpha}\right)\right] - \frac{by_v^*}{\alpha}\left(T_v - T_{\mathrm{ref}} + \frac{\delta T_y}{2}y_v^*\right)\ln Y_n + \frac{\mu_v}{\mu_{\mathrm{wall}}}\frac{C_1 y_v^*}{\alpha}(1 - b_\mu y_v^{*2})\ln Y_n + \frac{\mu_v}{\mu_{\mathrm{wall}}}\frac{C_1 y_v^{*2}}{2}\left(1 - b_\mu\frac{5y_v^{*2}}{6}\right) + \frac{\mu_v}{\mu_{\mathrm{wall}}}\frac{b(T_{\mathrm{wall}} - T_{\mathrm{ref}})y_v^{*2}}{2}\left(1 - b_\mu\frac{5y_v^{*2}}{6}\right) + \frac{\mu_v}{\mu_{\mathrm{wall}}}\frac{by_v^*}{\alpha}(T_{\mathrm{wall}} - T_{\mathrm{ref}})(1 - b_\mu y_v^{*2})\ln Y_n - \frac{\mu_v}{\mu_{\mathrm{wall}}}\frac{b(T_{\mathrm{wall}} - T_v)y_v^{*2}}{2}\left(\frac{1}{3} - b_\mu\frac{3y_v^{*2}}{10}\right) - \frac{\mu_v}{\mu_{\mathrm{wall}}}\frac{by_v^*(T_{\mathrm{wall}} - T_v)}{2\alpha}(1 - b_\mu y_v^{*2})\ln Y_n \quad \text{(B.11)}$$

$$Y_{Tn} = \left[1 + \alpha_t(y_n^* - y_v^*)\right],\ Y_n = \left[1 + \alpha(y_n^* - y_v^*)\right] \quad \text{and} \quad \delta T_y = \frac{T_v - T_n}{y_n^* - y_v^*} \quad \text{(B.12)}$$

Appendix C. Basic second-moment-closure model

The modelling of the pressure-redistribution terms ϕ_{ij} and the dissipation rate ε_{ij} of the stress components are the major differences between the two second-moment-closures. The pressure–strain correlation is often the most important term requiring modelling and is usually split into three parts:

$$\phi_{ij} = \phi_{ij1} + \phi_{ij2} + \phi_{ij3} \quad \text{(C.1)}$$

The first part is from turbulence-turbulence interactions (the ''slow pressure–strain'', ϕ_{ij1}), the second part involves mean strain terms (the ''rapid pressure–strain'', ϕ_{ij2}) and the third part is due to fluctuating force fields. The term ϕ_{ij1} is the so-called 'return to isotropy' term which redistributes the energy to reduce the anisotropy of the Reynolds stresses. It is modelled as proposed by Rotta (1951)

$$\phi_{ij1} = -\rho c_1 \varepsilon a_{ij} \quad \text{(C.2)}$$

where

$$a_{ij} = \frac{\overline{u_i u_j}}{k} - \frac{2}{3}\delta_{ij} \quad \text{(C.3)}$$

Similarly, the term ϕ_{ij2} tends to reduce the anisotropy of the stress production. A simple model for the ''rapid'' pressure strain term was proposed by Naot et al. (1970):

$$\phi_{ij2} = -c_2\left(P_{ij} - \frac{1}{3}P_{kk}\delta_{ij}\right) \quad \text{(C.4)}$$

Launder (1975) noted that in buoyant flows it was consistent to include buoyant stress production in a similar way to the expression for ϕ_{ij2}:

$$\phi_{ij3} = -c_3\left(G_{ij} - \frac{1}{3}G_{kk}\delta_{ij}\right) \quad \text{(C.5)}$$

The above terms do not take into account wall-effects. The wall causes a reflection of the turbulent pressure fluctuations, and this process forces the Reynolds stress normal to the wall to fall to zero much faster than those parallel to the wall. Since the standard expressions for the pressure-correlations do not account for this process, 'wall-reflection' terms are traditionally added to the overall pressure strain model, of the form:

$$\phi_{ij}^w = \phi_{ij1}^w + \phi_{ij2}^w$$

where a widely-used wall correction to the 'slow part' of pressure-correlation term proposed by Shir (1973) is

$$\phi^{w}_{ij1} = \rho c_{1w}\frac{\varepsilon}{k}\left(\overline{u_l u_m}n_l n_m\delta_{ij} - \frac{3}{2}\overline{u_i u_l}n_j n_l - \frac{3}{2}\overline{u_j u_l}n_i n_l\right)\left(\frac{l}{2.5y}\right) \tag{C.6}$$

and a contribution to the 'rapid part' proposed by Craft and Launder (1992) is

$$\begin{aligned}\phi^{w}_{ij2} = {} & -0.08\rho\frac{\partial U_l}{\partial x_m}\overline{u_l u_m}(\delta_{ij} - 3n_i n_j)\left(\frac{l}{2.5y}\right) \\ & - 0.1\rho k a_{lm}\left(\frac{\partial U_k}{\partial x_m}n_l n_k\delta_{ij} - \frac{3}{2}\frac{\partial U_i}{\partial x_m}n_l n_j - \frac{3}{2}\frac{\partial U_j}{\partial x_m}n_l n_i\right)\left(\frac{l}{2.5y}\right) + 0.4\rho k \\ & \times\frac{\partial U_l}{\partial x_m}n_l n_m\left(n_i n_j - \frac{1}{3}\delta_{ij}\right)\left(\frac{l}{2.5y}\right)\end{aligned} \tag{C.7}$$

In the above expressions n_l is the unit vector normal to the wall, l is the turbulence length scale and y is the distance from the wall. The various constants of the basic Reynolds-stress-model are: $c_1 = 1.8$; $c_2 = 0.6$; $c_3 = 0.5$; $c_{1w} = 0.5$. It should be noted that (inconsistently) there is no wall-reflection term associated with the buoyant contribution to the pressure strain. The last remaining term in the Reynolds-stress equations which needs to be modelled is the viscous dissipation rate ε_{ij} of the stress component. Often, the dissipation process is less significant than the pressure-redistribution terms and, commonly, local isotropy is assumed:

$$\varepsilon_{ij} = -2\nu\overline{\frac{\partial u_i}{\partial x_k}\frac{\partial u_j}{\partial x_k}} \approx \frac{2}{3}\varepsilon\delta_{ij} \tag{C.8}$$

Appendix D. Two-component-limit model

Although the basic second-moment-closure incorporates many important physical effects and, thus, in many cases is more general than any two-equation linear EVM, it still possesses a number of limitations. The first major drawback is associated with the use of the wall-normal unit vector n and shortest distance to the wall y that appear in the wall-reflection terms (C.6) and (C.7). These two quantities are mathematically and physically difficult to define in complex geometries. The second problem is that the pressure-correlation terms should tend to zero in the vicinity of the walls, next to free-surfaces or in regions of strong stable horizontal stratification, where one of the stress components vanishes. The basic Reynolds-stress model does not ensure this and thus will not necessarily perform well in situations where the turbulence approaches a two-component state (Lumley, 1978). To overcome these problems, the UMIST group following the general strategy of Shih and Lumley (1985) developed the so-called TCL model—a pressure–strain model which strictly satisfies the two-component-limit behaviour. The great advantage of the TCL model is that there is no need for additional wall-reflection terms, and accordingly one does not need to define wall-normal vectors and distances to the wall. In ensuring that ϕ_{ij} vanishes if the corresponding normal stress becomes zero, the model is also realisable, meaning that it cannot produce unrealistic negative values for the normal stresses. In the TCL model the 'return to isotropy' term ϕ_{ij1} is different from that in the basic second-moment-closure model (C.2). Some researchers have pointed out that the basic linear model of the ϕ_{ij1} term given by Eq. (C.2) is not really appropriate for a non-linear process. Instead Lumley (1978), Reynolds (1984) and Fu (1988) suggested non-linear versions of ϕ_{ij1}. Finally the TCL model adopted the expression recommended by Craft et al. (1989):

$$\phi_{ij1} = -\rho c_1\varepsilon\left[a_{ij} + c_1'(a_{ik}a_{jk} - 1/3A_2\delta_{ij})\right] - A^{0.5}\varepsilon a_{ij} \tag{D.1}$$

The ϕ_{ij2} term of the TCL model was initially proposed by Fu (1988), who ensured the correct behaviour of the term as one of the fluctuating velocity components vanishes:

$$\begin{aligned}\phi_{ij2} = {} & -0.6\left(P_{ij} - \frac{1}{3}P_{kk}\delta_{ij}\right) + 0.3\varepsilon a_{ij}(P_{kk}/\varepsilon) - 0.2\rho\left[\frac{\overline{u_k u_j u_l u_i}}{k}\left(\frac{\partial U_k}{\partial x_l} + \frac{\partial U_l}{\partial x_k}\right) - \frac{\overline{u_l u_k}}{k}\left(\overline{u_i u_k}\frac{\partial U_j}{\partial x_l} + \overline{u_j u_k}\frac{\partial U_i}{\partial x_l}\right)\right] \\ & - c_2\left[A_2(P_{ij} - D_{ij}) + 3a_{mi}a_{nj}(P_{mn} - D_{mn})\right] + c_2'\left\{\left(\frac{7}{15} - \frac{A_2}{4}\right)\left(P_{ij} - \frac{1}{3}\delta_{ij}P_{kk}\right) + 0.1\varepsilon\left[a_{ij} - \frac{1}{2}\left(a_{ik}a_{kj} - \frac{1}{3}\delta_{ij}A_2\right)\right](P_{kk}/\varepsilon)\right. \\ & - 0.05a_{ij}a_{lk}P_{kl} + 0.1\left[\left(\frac{\overline{u_i u_m}}{k}P_{mj} + \frac{\overline{u_j u_m}}{k}P_{mi}\right) - \frac{2}{3}\delta_{ij}\frac{\overline{u_l u_m}}{k}P_{ml}\right] + 0.1\left[\frac{\overline{u_k u_j u_l u_i}}{k^2} - \frac{1}{3}\delta_{ij}\frac{\overline{u_l u_m u_k u_m}}{k^2}\right] \\ & \left.\times\left[6D_{lk} + 13\rho k\left(\frac{\partial U_k}{\partial x_l} + \frac{\partial U_l}{\partial x_k}\right)\right] + 0.2\frac{\overline{u_k u_j u_l u_i}}{k^2}(D_{lk} - P_{lk})\right\}\end{aligned} \tag{D.2}$$

The model constants appearing in the expressions (D.1) and (D.2) have been taken as proposed by Craft (1998): $c_1 = 3.1 f_A \min[A_2; 0.5]$; $c_1' = 1.1$; $c_2 = \min\left[0.55; \frac{3.2A}{1+S}\right]$; $c_2' = \min[0.6; A] + \frac{2(S-\Omega)}{(3+S+\Omega)} - 1.5 S_I$ where

$$f_A = \begin{cases} A\left(\frac{0.05}{0.7}\right)^{0.5} & \text{for } A < 0.05 \\ \frac{A}{\sqrt{0.7}} & \text{for } 0.05 < A < 0.7 \\ A & \text{for } A > 0.7 \end{cases} \tag{D.3}$$

$$D_{ij} = -\rho\left(\overline{u_i u_k}\frac{\partial U_k}{\partial x_j} + \overline{u_j u_k}\frac{\partial U_k}{\partial x_i}\right) \tag{D.4}$$

$$S = \frac{k}{\varepsilon}\left(\frac{1}{2} S_{ij} S_{ij}\right)^{1/2} \tag{D.5}$$

$$S_{ij} = \frac{\partial U_i}{\partial x_j} + \frac{\partial U_j}{\partial x_i} \tag{D.6}$$

$$S_I = \frac{S_{ij} S_{jk} S_{ki}}{\sqrt[3]{S_{lm} S_{ml}}} \tag{D.7}$$

$$\Omega = \frac{k}{\varepsilon}\left(\frac{1}{2}\Omega_{ij}\Omega_{ij}\right)^{1/2} \tag{D.8}$$

$$\Omega_{ij} = \frac{\partial U_i}{\partial x_j} - \frac{\partial U_j}{\partial x_i} \tag{D.9}$$

In addition to the above expressions for ϕ_{ij1} and ϕ_{ij2} the buoyant contributions to ϕ_{ij} are accounted for in the expression ϕ_{ij3} as suggested by Craft (1991):

$$\begin{aligned}
\phi_{ij3} = &-\left(\frac{4}{10} - \frac{3}{80}A_2\right)\left(G_{ij} - \frac{1}{3}\delta_{ij}G_{kk}\right) + \frac{1}{4}a_{ij}G_{kk} \\
&+ \frac{3}{20}\rho\left(\beta_i\frac{\overline{u_m u_j}}{k} + \beta_j\frac{\overline{u_m u_i}}{k}\right)\overline{u_m\theta} - \frac{1}{10}\rho\delta_{ij}\beta_k\frac{\overline{u_m u_k}}{k}\overline{u_m\theta} \\
&- \frac{1}{4}\rho\beta_k\left(\frac{\overline{u_k u_i}}{k}\overline{u_j\theta} + \frac{\overline{u_k u_j}}{k}\overline{u_i\theta}\right) \\
&+ \frac{1}{20}\rho\delta_{ij}\beta_k\frac{\overline{u_m u_n u_m u_k}}{k^2}\overline{u_n\theta} \\
&- \frac{1}{8}\rho\left(\frac{\overline{u_m u_j}}{k}\overline{u_i\theta} + \frac{\overline{u_m u_i}}{k}\overline{u_j\theta}\right)\frac{\overline{u_m u_k}}{k}\beta_k \\
&+ \frac{1}{8}\rho\left(\frac{\overline{u_k u_i u_m u_j}}{k^2} + \frac{\overline{u_k u_j u_m u_i}}{k^2}\right)\beta_k\overline{u_m\theta} \\
&+ \frac{3}{40}\rho\left(\beta_i\frac{\overline{u_m u_j}}{k} + \beta_j\frac{\overline{u_m u_i}}{k}\right)\frac{\overline{u_m u_n}}{k}\overline{u_n\theta} \\
&+ \frac{1}{4}\rho\beta_k\frac{\overline{u_m u_k u_i u_j}}{k^2}\overline{u_m\theta}
\end{aligned} \tag{D.10}$$

The above pressure-correlation terms are not the only advantages of the TCL model. Perot and Moin (1995), after processing their DNS data, acknowledged that the isotropic assumption for the dissipation rate of the stress components (C.8) is not valid in many situations—especially next to free surfaces and solid walls. Therefore, in the TCL closure, the viscous dissipation rate of the stresses is modelled in a more elaborate way, similar to that suggested by Craft and Launder (1996):

$$\varepsilon_{ij} = \frac{(1-A)}{D}\left(\varepsilon_{ij}' + \varepsilon_{ij}''\right) + \frac{2}{3}A\delta_{ij}\varepsilon \tag{D.11}$$

where

$$\begin{aligned}
\varepsilon_{ij}' = &\frac{\varepsilon}{k}\overline{u_i u_j} + 2\nu\frac{\overline{u_l u_n}}{k}\frac{\partial\sqrt{k}}{\partial x_l}\frac{\partial\sqrt{k}}{\partial x_n}\delta_{ij} + 2\nu\frac{\overline{u_l u_i}}{k}\frac{\partial\sqrt{k}}{\partial x_j}\frac{\partial\sqrt{k}}{\partial x_l} \\
&+ 2\nu\frac{\overline{u_l u_j}}{k}\frac{\partial\sqrt{k}}{\partial x_i}\frac{\partial\sqrt{k}}{\partial x_l}
\end{aligned}$$

and

$$\varepsilon_{ij}'' = \varepsilon\left[2\frac{\overline{u_l u_k}}{k}d_l^a d_k^a\delta_{ij} - \frac{\overline{u_l u_i}}{k}d_l^a d_j^a - \frac{\overline{u_l u_j}}{k}d_l^a d_i^a\right](1-A)$$

$$D = \frac{(\varepsilon_{kk}' + \varepsilon_{kk}'')}{2\varepsilon}, \quad d_i^a = \frac{N_i}{0.5 + (N_k N_k)^{0.5}},$$

$$N_i = \frac{\partial}{\partial x_i}\left[\frac{k^{3/2}A^{1/2}}{\varepsilon}\right]$$

It is finally noted that in the model of Craft and Launder (2002) similar TCL approximations were developed for the corresponding pressure-fluctuation terms in the transport equation for $\overline{u_j\theta}$. In the present work, however, the heat flux for both second-moment closures has been obtained much more simply from Eq. (3.25). It remains a task for the future to ascertain whether, with the more complete model for the heat fluxes, stability and accuracy may be further improved.

References

Addad, Y., Benhamadouche, S., Laurence, D., 2004. The negatively buoyant wall jet: LES results, International Journal of Heat and Fluid Flow 25 [this issue], doi:10.1016/j.ijheatfluidflow.2004.05.008.

Chieng, C.C., Launder, B.E., 1980. On the calculation of turbulent heat transfer downstream from an abrupt pipe expansion. Numerical Heat Transfer 3, 189–207.

Cotton, M.A., Jackson, J.D., 1987. Calculation of turbulent mixed convection in a vertical tube using a low-Reynolds-number k–ε turbulence model. In: Proceedings of the 6th Symposium on Turbulent Shear Flows, Toulouse.

Craft, T.J., 1991. Second-moment modelling of turbulent scalar transport. Ph.D. thesis, UMIST.

Craft, T.J., 1998. Developments in a low-Reynolds-number second-moment-closure and its application to separating and reattaching flows. International Journal of Heat and Fluid Flow 19, 541–548.

Craft, T.J., Fu, S., Launder, B.E., Tselepidakis, D.P., 1989. Developments in modelling the turbulent second-moment pressure correlations. Technical Report TFD/89/1, Department of Mechanical Engineering, UMIST.

Craft, T.J., Gerasimov, A.V., Iacovides, H., Launder, B.E., 2002. Progress in the generalization of wall-function treatments. International Journal of Heat and Fluid Flow 23 (2), 148–160.

Craft, T.J., Gerasimov, A.V., Iacovides, H., Launder, B.E., 2003. A new wall-function strategy applied to mixed convection in vertical annular passages. In: Proceedings of the Conference on Modelling Fluid Flow, The 12th International Conference on Fluid Flow Technologies, Budapest, Hungary.

Craft, T.J., Launder, B.E., 1992. New wall-reflection model applied to the turbulent impinging jet. AIAA Journal 30 (12), 2970–2972.

Craft, T.J., Launder, B.E., 1996. A Reynods stress closure designed for complex geometries. International Journal of Heat and Fluid Flow 17, 245–254.

Craft, T.J., Launder, B.E., 2001a. Applications of TCL modelling strategy in engineering and environmental flows. In: Proceedings of the 2nd International Symposium on Advances in Computational Heat Transfer, Queensland, Australia.

Craft, T.J., Launder, B.E., 2001b. On the spreading mechanism of the three-dimensional turbulent wall jet. Journal of Fluid Mechanics 435, 305–326.

Craft, T.J., Launder, B.E., 2002. Application of TCL modelling to stratified flows. In: Launder, B.E., Sandham, N. (Eds.), Closure Strategies for Turbulent and Transitional Flows. CUP, pp. 407–423.

Daly, B.J., Harlow, F.H., 1970. Transport equations in turbulence. Physics of Fluids 13, 2634–2649.

Fu, S., 1988. Computational modelling of turbulent swirling flows with second-moment closures. Ph.D. thesis, Faculty of Technology, University of Manchester.

Gibson, M.M., Launder, B.E., 1978. Ground effects on pressure fluctuations in the atmospheric boundary layer. Journal of Fluid Mechanics 86, 491–511.

He, S., Xu, Z., Jackson, J.D., 2002. An experimental investigation of buoyancy-opposed wall jet flow. International Journal of Heat and Fluid Flow 23, 487–496.

Huang, P.G., Leschziner, M.A., 1983. An introduction and guide to the computer code TEAM. Technical Report TF/83/9, Department of Mechanical Engineering, UMIST.

Jones, W.P., Launder, B.E., 1972. The prediction of laminarization with a two-equation model of turbulence. International Journal of Heat and Mass Transfer 15, 301–314.

Kline, S.J., Cantwell, B.J., Lilley, G.M., 1981. Proceedings of 1980-81 AFOSR-HTTM Stanford Conference on Complex Turbulent Flow, vol. 1, p. 439, Stanford.

Launder, B.E., 1975. On the effects of a gravitational field on the turbulent transport of heat and momentum. Journal of Fluid Mechanics 67, 569–581.

Launder, B.E., Rodi, W., 1981. The turbulent wall jet. Progress in Aerospace Sciences 19, 81–128.

Launder, B.E., Rodi, W., 1983. The turbulent wall jet—measurements and modelling. Annual Review of Fluid Mechanics 15, 429–459.

Launder, B.E., Sharma, B.I., 1974. Application of the energy-dissipation model of turbulence to the calculation of flow near a spinning disc. Letters in Heat and Mass Transfer 1, 131–138.

Launder, B.E., Spalding, D.B., 1974. The numerical computation of turbulent flows. Computer Methods in Applied Mechanics and Engineering 3, 269–289.

Lumley, J.L., 1978. Computational modelling of turbulent flows. Advances in Applied Mechanics 18, 123–175.

Naot, D., Shavit, A., Wolfshtein, M., 1970. Interactions between components of the turbulent velocity correlation tensor. Israel Journal of Technology 8, 259–269.

Perot, J.B., Moin, P., 1995. Shear-free turbulent boundary layers. Part 2: New concepts for Reynolds-stress-transport equation modelling of inhomogeneous flows. Journal of Fluid Mechanics 295, 229–245.

Reynolds W.C., Physical and analytical foundations, concepts and new directions in turbulence modelling and simulation, in: Turbulence Models and their Applications-2, Eyrolles, Paris, 1984.

Rotta, J.C., 1951. Statistische theorie nichthomogener turbulenz. Zeitschrift für Physik 129, 547–572.

Shih, T.H., Lumley, J.L., 1985. Modelling of pressure-correlation terms in Reynolds stress and scalar flux equations. Technical Report FD-85-03, Sibley School of Mechanical and Aerospace Engineering, Cornell University.

Shir, C.C., 1973. A preliminary numerical study of atmospheric turbulent flows in the idealized planetary boundary layer. Journal of Atmospheric Sciences 30, 1327–1339.